ME 388F Homework 5

Erik Hansen

March 10, 2025

See my GitHub repository s25me388f_hansen in the folder hw5 for the code used below. Plots were generated on simplified Monte Carlo output from part1.py and on the order of convergence from part2.py.

1 Simplified Monte Carlo

1.1 One Random Number in Source Free Transport

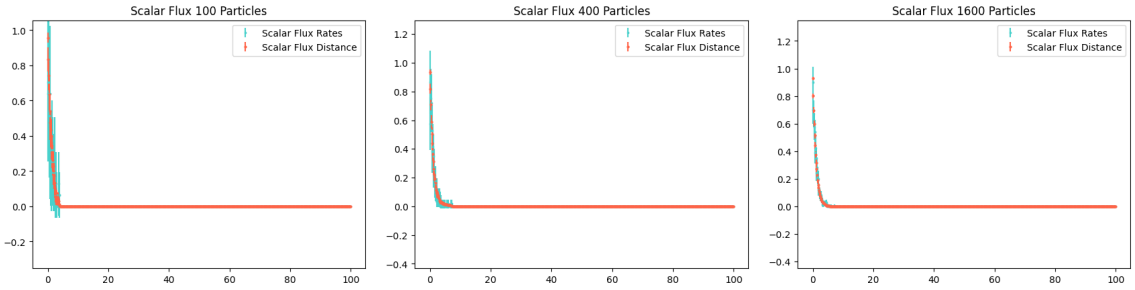

Figure 1: Rightward flux into a sourcefree medium with $\Sigma_t = 1$, no scattering, and $\mu = 1$. Plots are shown with particle numbers $N_p = 100$, $N_p = 400$, and $N_p = 1600$ in a mesh with 640 cells. We observe convergence towards the exponentially decreasing analytic solution from $\phi = 1$. The size of the scalar flux from reaction tally error bars between plots and observe that the size of the error roughly halves between plots, which is consistent with the factor of four increase in particle histories. This appears to also be the case for the scalar flux from track length tallies.

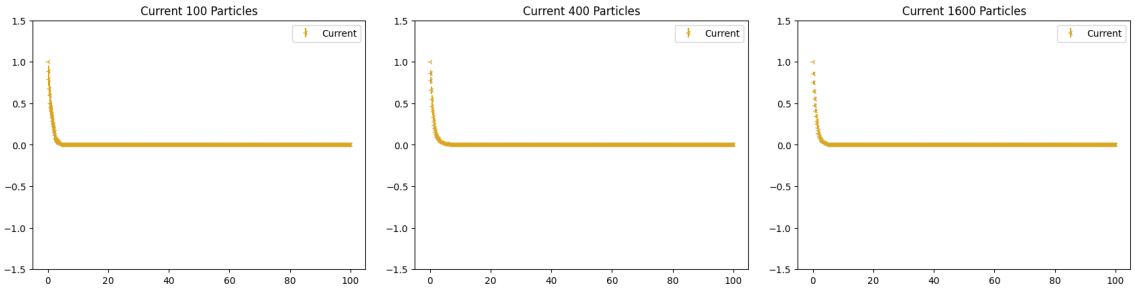

Figure 2: Current in above $\mu = 1$ flux into a sourcefree absorber. We see an expected exponential decrease in current. The rate of convergence in the current is similar to the convergence in the track length tallies.

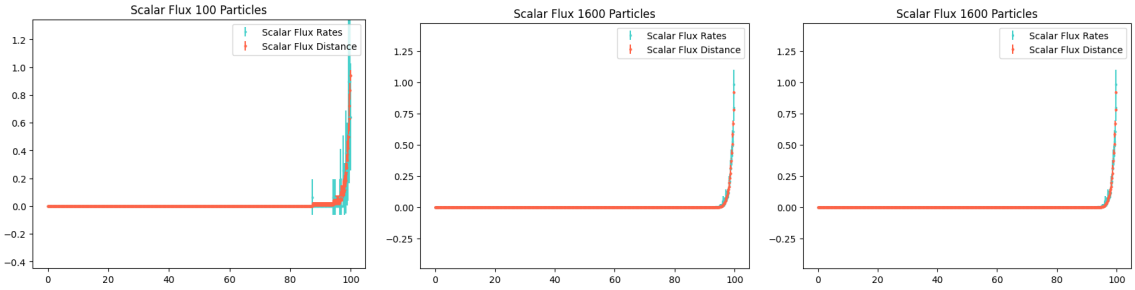

Figure 3: Leftward flux into a sourcefree medium with $\Sigma_t = 1$, no scattering, and $\mu = -1$. We again see the expected convergence towards an exponentially decreasing solution as x decreases, and halving of the error bars as the number of grid cells quadruples.

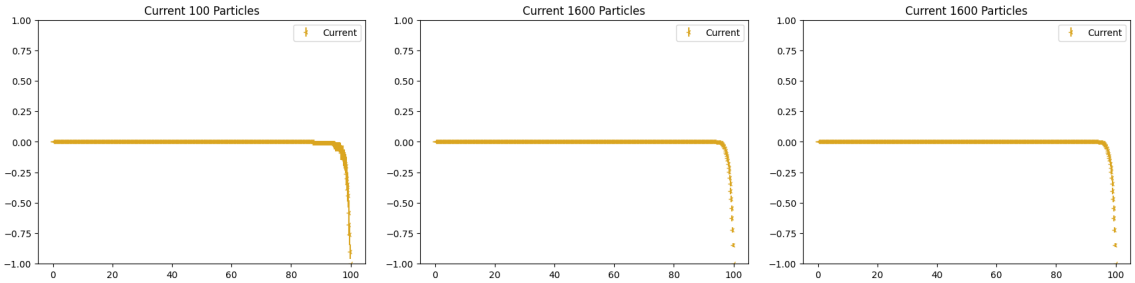

Figure 4: Current in flux into a sourcefree medium with $\mu = -1$. We again see the expected convergence towards an exponentially decreasing solution as x decreases, and halving of the error bars as the number of grid cells quadruples.

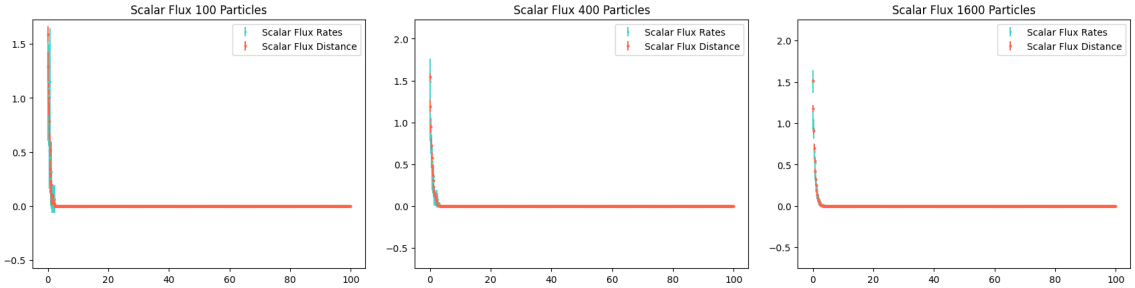

Figure 5: Scalar flux with $\mu = \frac{1}{\sqrt{3}}$ incident neutrons. We notice the steeper decline in the exponential due to the increase in the decay constant $\tau = \frac{\Sigma_t}{\mu}$. However, this appears to be off by a numerical factor of $\sqrt{3}$ due to the change in μ. We continue to see that the error scales as $N^{-1/2}$, however.

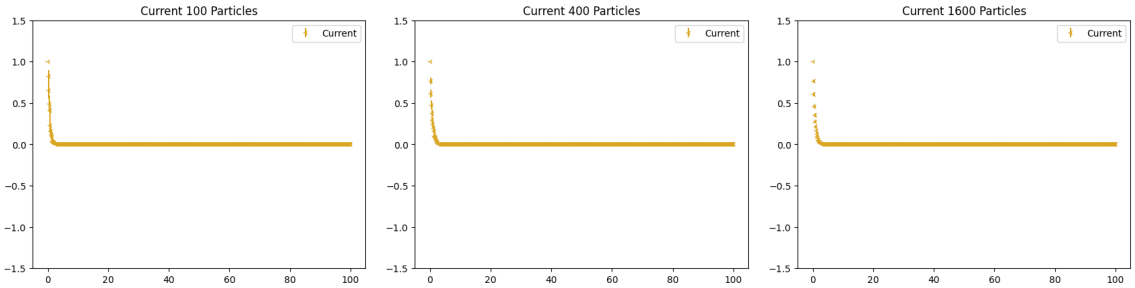

Figure 6: Current corresponding to the $\mu = \frac{1}{\sqrt{3}}$ scalar flux. This shows a current with exponential decay and a larger decay constant than $\mu = 1$, as expected. We continue to see the rate of increase similar to the convergence of the track length tally scalar flux.

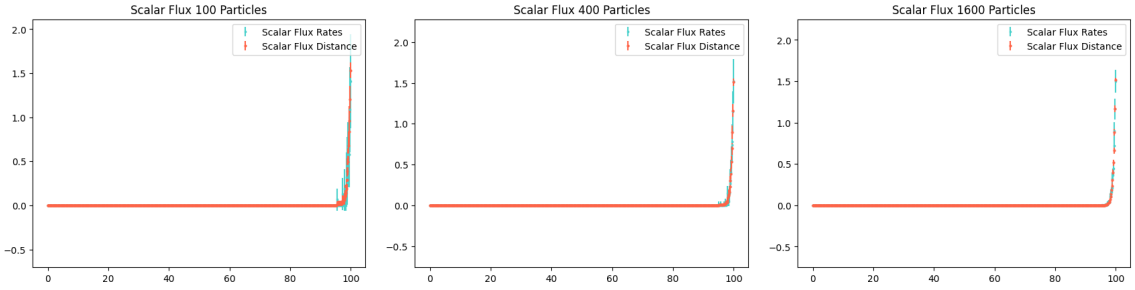

Figure 7: Scalar flux for a $\mu = -\frac{1}{\sqrt{3}}$ beam. We see that this solution is the mirror image of the case above, where we have similarly sized error bars throughout and a similarly enhanced rate of decrease. We also note that the scalar flux we found has the same amplitude as the $+\frac{1}{\sqrt{3}}$ beam, suggesting that there is a normalization issue related to the direction of the beam.

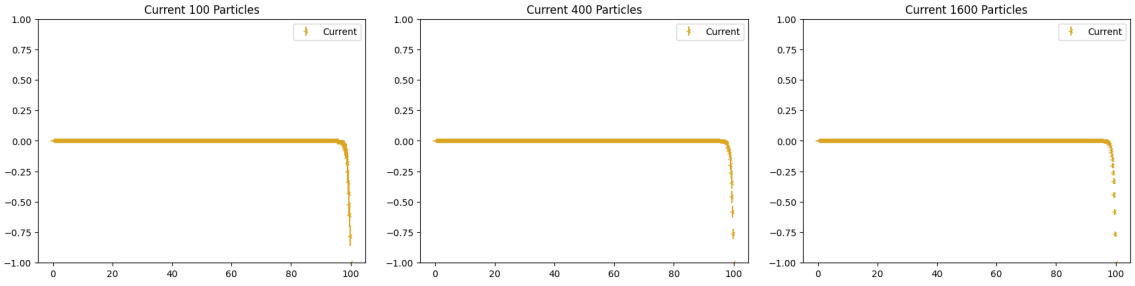

Figure 8: We see the current for $\mu = -\frac{1}{\sqrt{3}}$ flux into a source free absorber. It's shape is opposite to the scalar flux found in 7. We notice that this current is only slightly less than the predicted limiting value of -1 before increasing to zero at the same increased rate for smaller $|\mu|$. The rate of error decrease is similar to previous cases.

1.2 Three Random Numbers in Isotropic Source Reflectors

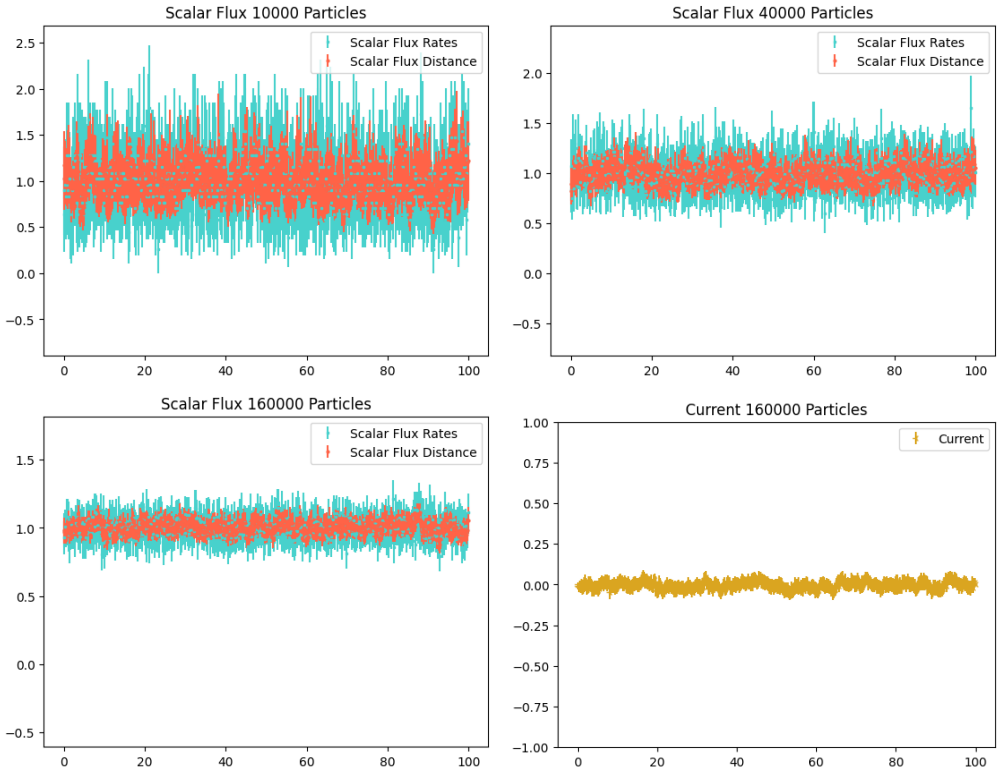

Figure 9: Scalar flux and current in a system with isotropic source and reflecting boundary conditions, with 10^4, $4 * 10^4$, and $1.6 * 10^5$ particle histories. We see that the solution is approximately flat in all cases, the current is zero, the error and spread of the scalar flux halves as the number of particle histories quadruples, and that the value of the scalar flux agrees with that we would expect, $\frac{Q}{\Sigma_a} = \frac{1}{1} = 1$.

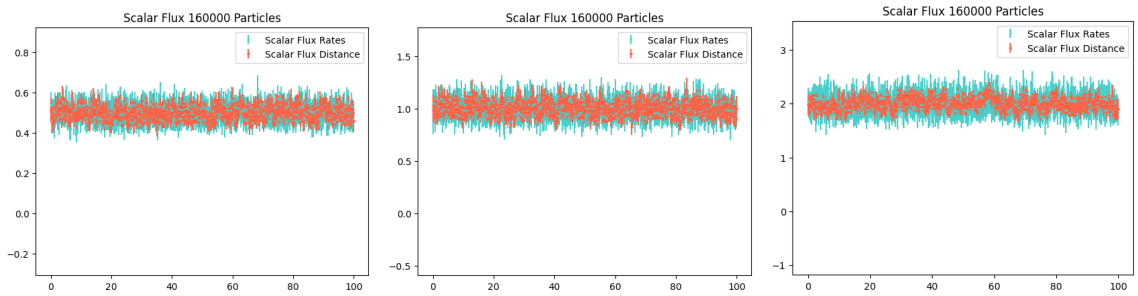

Figure 10: Scalar flux in reflecting boundary conditions and no scattering with varying sources $Q = 1, 2, 2$ and transport cross section $\Sigma_t = \Sigma_a = 2, 2, 1$, respectively. We see that when Σ_t doubles, the scalar flux halves on the left, and with the source doubling, the scalar flux doubles on the right, as predicted.

1.3 Two Random Numbers in Source Free Transport

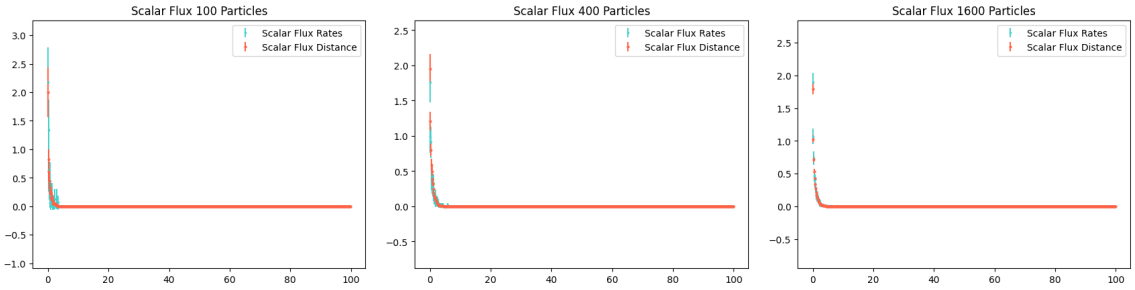

Figure 11: Scalar flux in forward incident beam with sampled angle for $100, 400$, and 1600 particle histories. We see that as the number of particle histories increases, the error decreases as expected, and the scalar flux due to the reaction rate follows the exponential pattern as expected. This follows the same form as a discrete ordinates solution shown later, but fails to have the same amplitude. This is likely due to a normalization issue involving different values of the sampled angle.

2 Order of Convergence

For each problem discussed, we show the solution for the highest resolution spatial mesh or particle histories and a plot of the L_2 error in lower spatial mesh or We also have produced plots available in full from the Github repository, and highlight the most significant results regarding the order of convergence estimates. All plots of solutions for the different grid resolutions are available in the GitHub repository. All discrete ordinate solutions shown use 64 discrete ordinates and all Monte Carlo solutions use 200 spatial cells. The diffusion codes use Marshak boundary conditions in all cases, unless specified as reflecting.

2.1 Isotropic Flux on One Surface

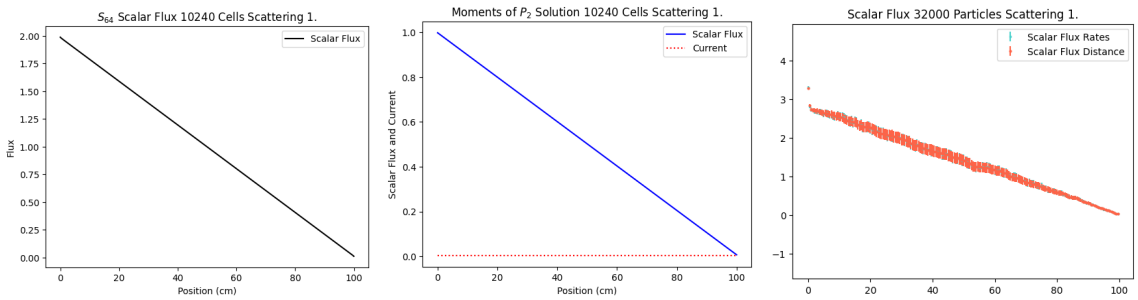

Figure 12: Best discrete ordinates, diffusion, and Monte Carlo solutions for an incident beam into a fully scattering $\Sigma_s = 1$ source free region. We see that the diffusion and discrete ordinates solution have the same shape, but the discrete ordinate solution has double the magnitude of scalar flux, which the correct analytical solution. The Monte Carlo method also shows a linear increase, but shows some effects of curvature near the incoming boundary and overshoots the correct value of the scalar flux.

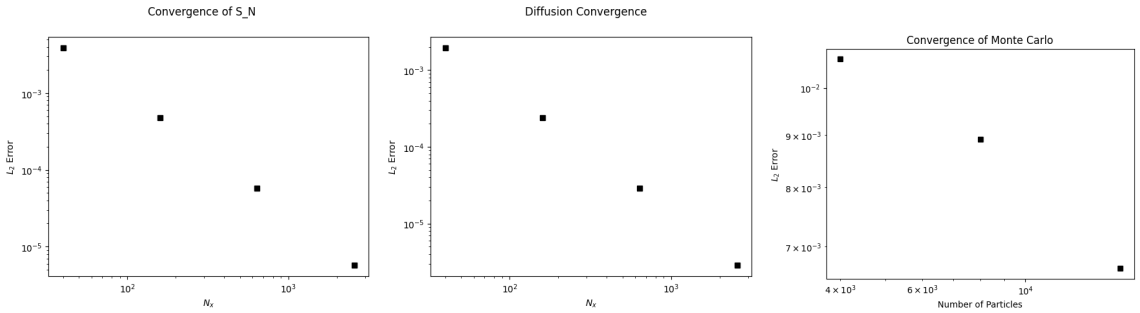

Figure 13: We use a log-log plot of the L_2 discrepancy between the scalar fluxes obtained for discrete ordinate, diffusion, and Monte Carlo solutions between a best and worse resolved mesh. The L_2 difference is taken between the higher resolved solution at the left edge of the cells of the worse resolved plot. The discrete ordinate and diffusion convergence plots take this form in all cases, so we only discuss their rate of convergence here. We notice that between each simulation, the spatial mesh increases a factor of four, and the error falls a factor of four. This suggests that the diffusion and discrete ordinates code share a first order of convergence. This is likely determined by the use of diamond difference in calculations, and why we would not instantly achieve a correct answer as step characteristics. We also see that the Monte Carlo simulations with smaller particle histories show that on average, between the smallest and largest errors displayed, as the number of particles is quadrupled, the error is halved. This suggests an order of convergence of 1/2, as required from the error estimate of a Monte Carlo simulation.

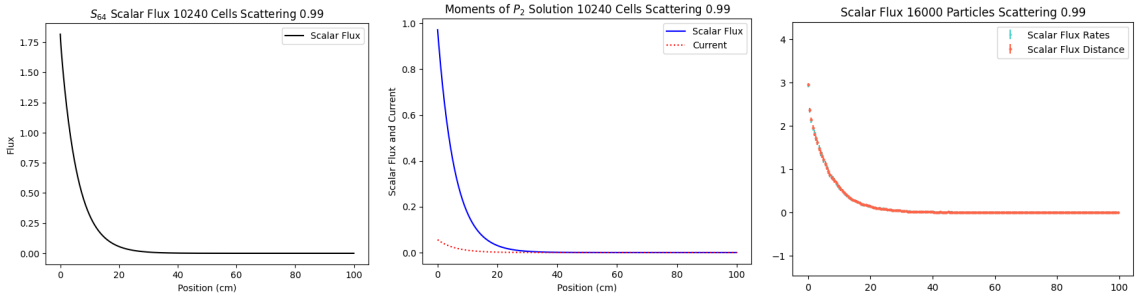

Figure 14: Entrance into a $\Sigma_s = 0.9$ in $\Sigma_t = 1$ medium. We find an exponential decrease in the scalar flux with distance, as expected. The diffusion solution underestimates the scalar flux at the boundary and the Monte Carlo simulation again overestimates it.

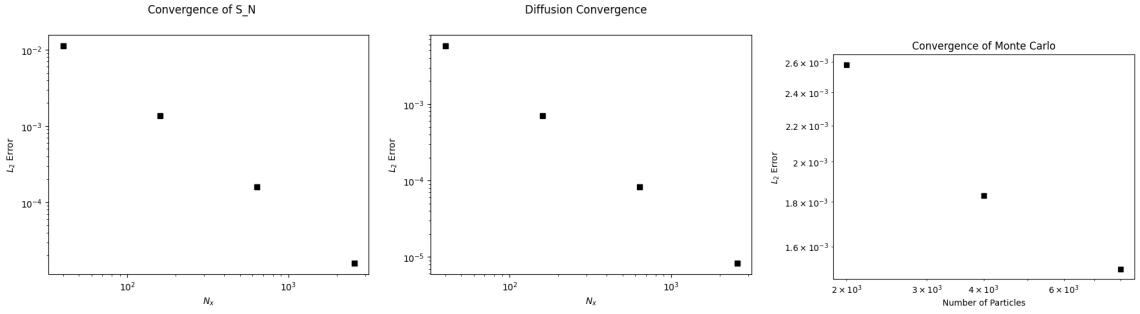

Figure 15: The convergence properties of all three simulations follow the same pattern as above.

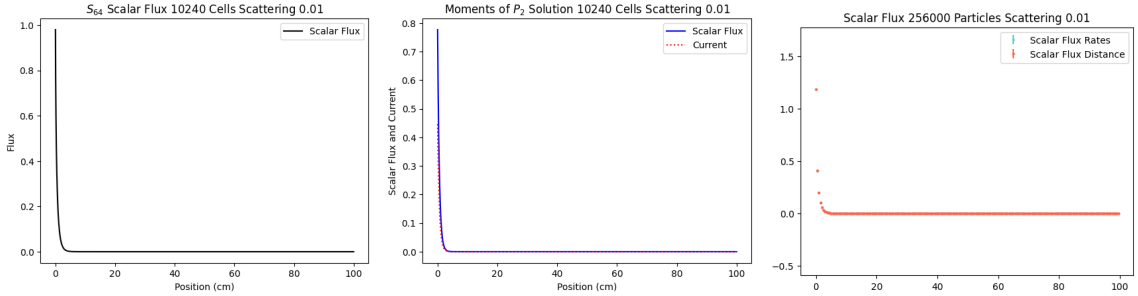

Figure 16: We find that the exponential decrease shown with $\Sigma_s = 0.99$ has sharpened to a rapid decrease. The discrete ordinates code decreases from one rapidly, matching the analytic solution. The diffusion code shows a similar decrease but with slightly less flux, and the Monte Carlo simulation as discussed earlier overestimates the solution.

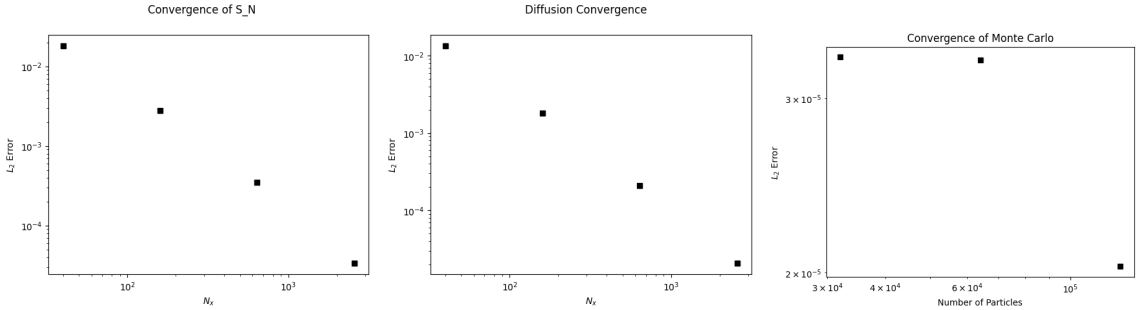

Figure 17: We see that our best simulation is about as accurate as the other particle histories and we only just see convergence towards them. This could suggest that this case requires more particles to do an accurate convergence study.

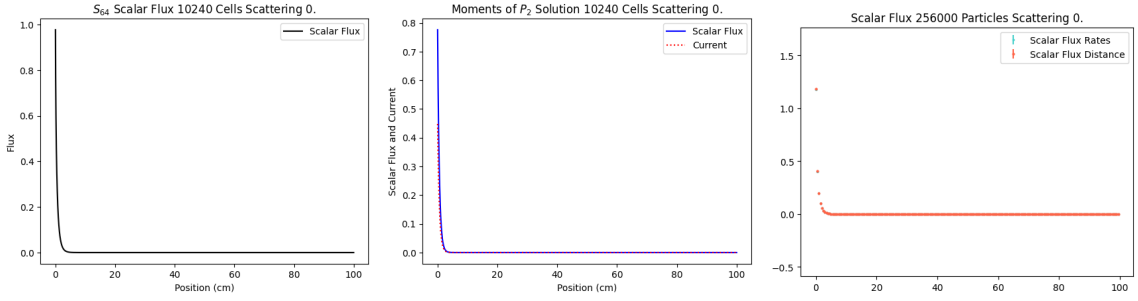

Figure 18: We now recover the angular flux studied earlier in our simplified Monte Carlo Method. However, this case is indistinguishable from the $\Sigma_s = 0.01$ case.

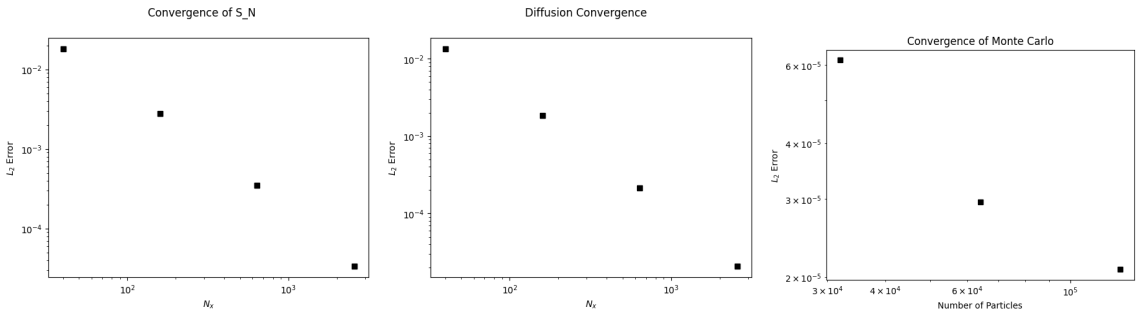

Figure 19: Here we see that the Monte Carlo simulation error is again small, but we have a clear decrease across the simulations which supports a one-half order of convergence.

2.2 Isotropic Source with Vacuum Boundary

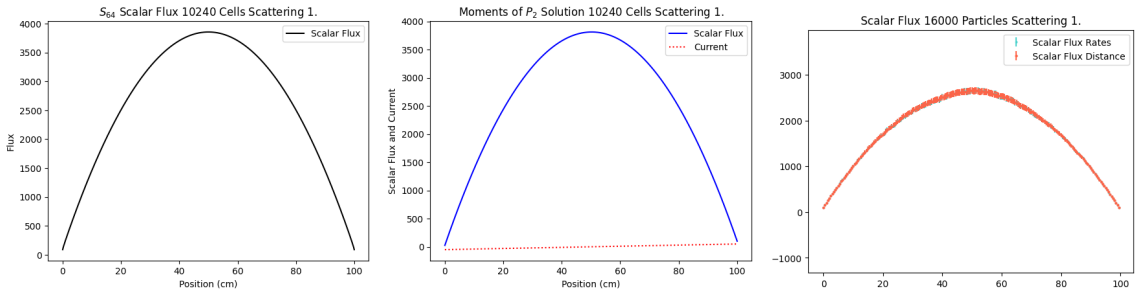

Figure 20: Here we see an isotropic source with full scattering ratio $\Sigma_t = \Sigma_s = 1$ surrounded by a vacuum as simulated by all three methods. Both the diffusion and discrete ordinates codes find an analytical solution of a cosine wave (explanation thanks to Harrison Reisinger). However, the Monte Carlo method shows a similar shape but underestimates the solution by a factor of roughly $\frac{3}{4}$.

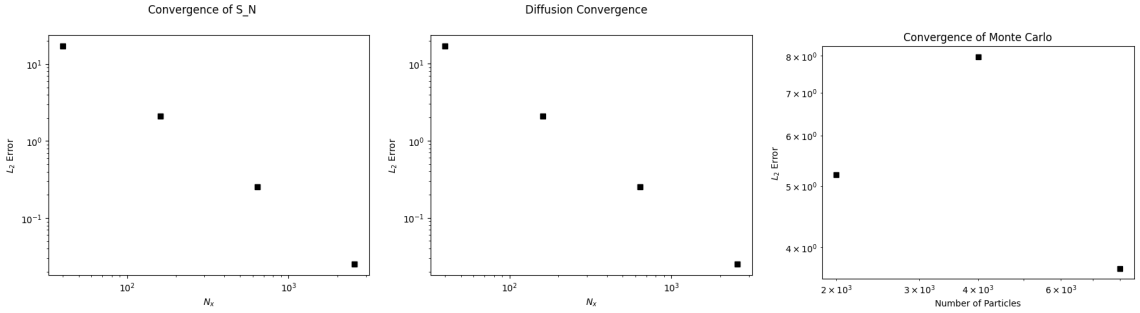

Figure 21: Here we see that even though the error in the different particle histories is fairly small relative to the size of the scalar flux, we don't see continuous decrease in the error yet. This likely means we need to simulate with more particle histories for our best solution, which is expensive in this case since particles only leave the system through boundaries.

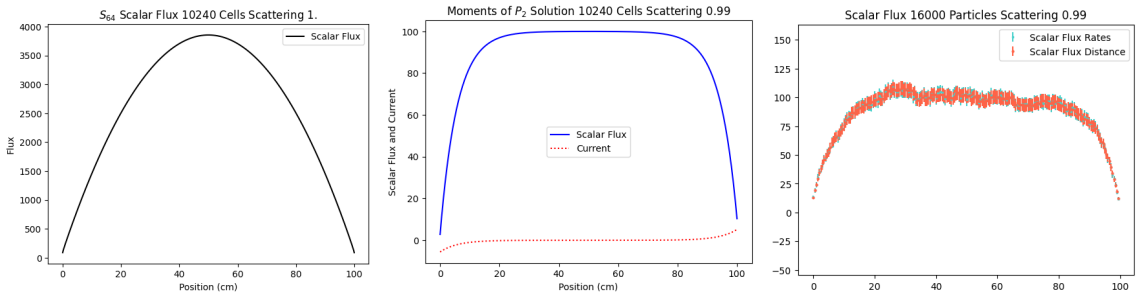

Figure 22: With scattering reduced to $\Sigma_s = 0.99$, the discrete ordinates and diffusion codes form a plateau with a peak at 100 as in the infinite homogeneous problem. The Monte Carlo method reaches the same peak, but fails to become flat.

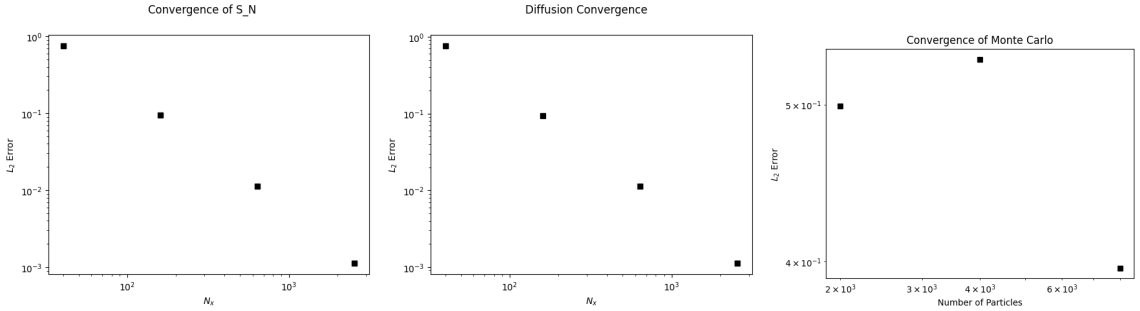

Figure 23: We see that both deterministic methods retain their roughly order one convergence, but the Monte Carlo method hasn't been resolved enough for use in determining the order of convergence in this case.

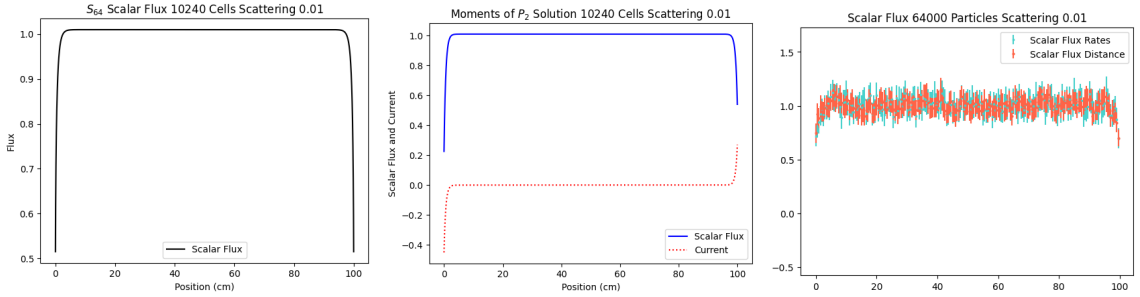

Figure 24: In the limit of small scattering, all methods show a decrease to the vacuum boundary but an interior value slightly above one, consistent with the analytical solution $\frac{Q}{\Sigma_a}$.

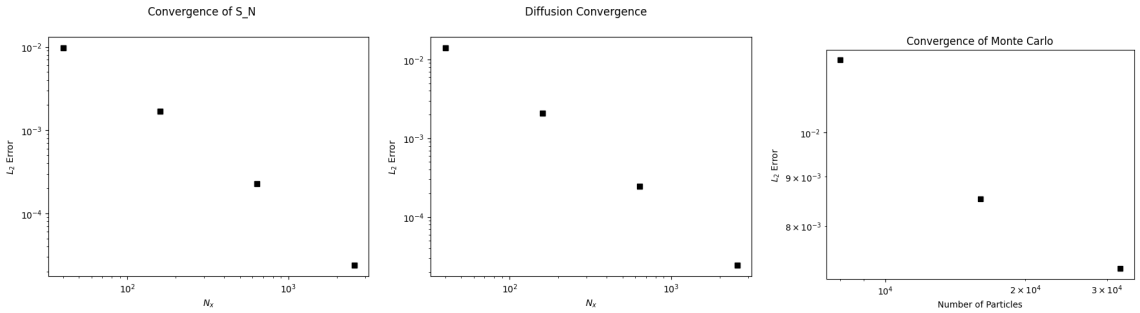

Figure 25: With the limit of low scattering, we find that the Monte Carlo method shows its order half convergence.

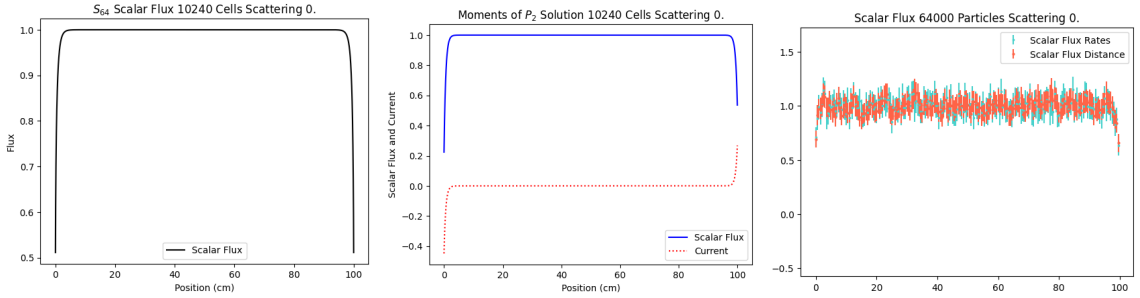

Figure 26: With no scattering, we return to the infinite homogeneous problem, and all three methods show a vacuum boundary and an interior flux of 1.

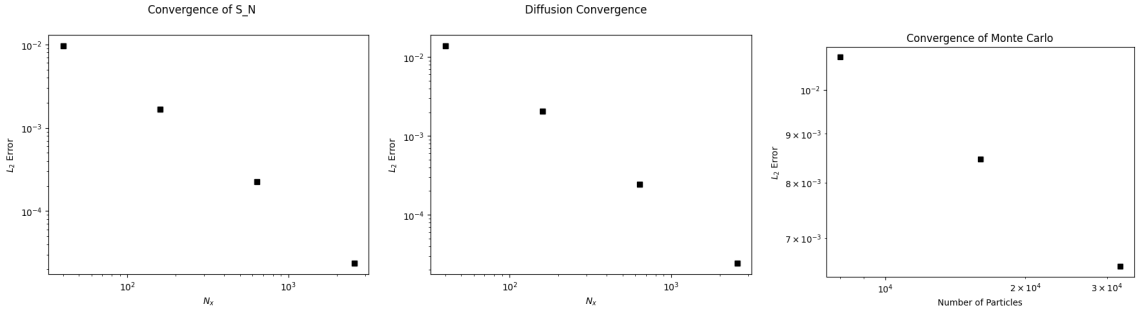

Figure 27: All methods converge as expected in this limit.

2.3 Multimaterial Reactor Configurations

We choose to study an absorber/air system with backwards flux $1 neutron/(cm^2 s\mu)$ on the right boundary, a vacuum boundary on the left, with a $20cm$ absorber and $80cm$ air.

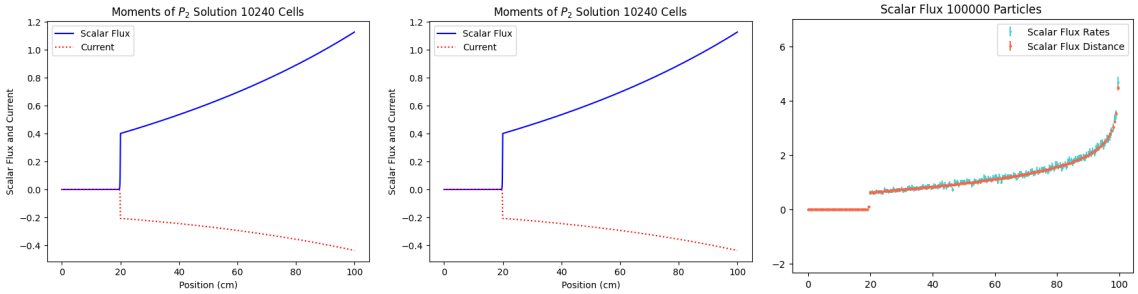

Figure 28: As we may expect, we see a gradual decrease in the flow coming in the right side, followed by an abrupt decrease in the flux due to the absorber. (This was chosen as a test of an analytic scenario where the transport cross section changes between materials, which the diffusion and ordinates solution attain). We see similar behavior in the Monte Carlo simulation, but it overestimates the solution.

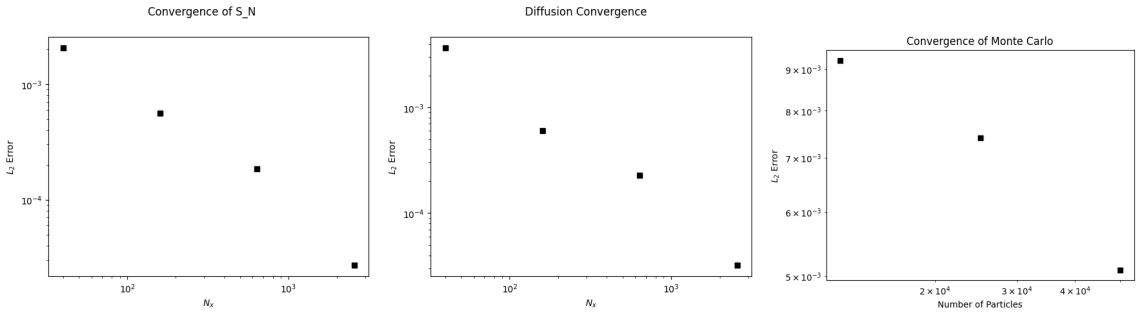

Figure 29: We see both orders of convergence represented well here. The error in the deterministic methods decreases by a factor of about 100 as the mesh size increases by 64, leading to an order of convergence of one. On the other hand, the error in the Monte Carlo simulation decreases by just less than half when the number of histories is quadrupled, consistent with an order $\frac{1}{2}$ convergence.

We also study a source/reflector system with no incoming flux at left but reflecting boundary conditions at right.

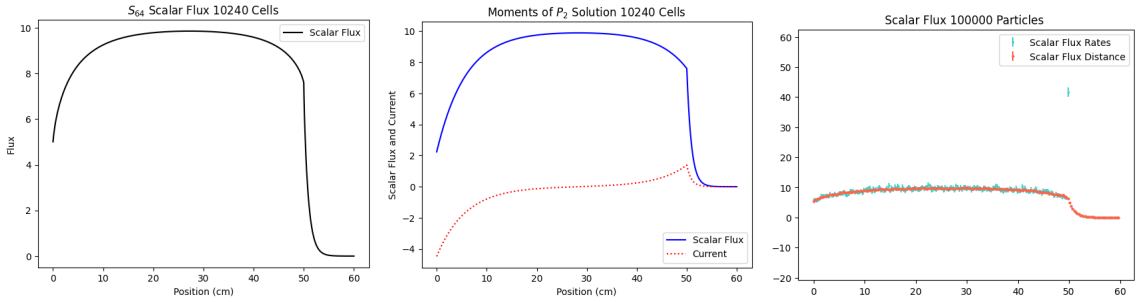

Figure 30: Again we find a distribution as expected. Like in the vacuum boundary surrounding a source, we find a scalar flux that decreases to zero on both sides of the source. However, the reflector causes the current to be zero at the right boundary and so the decrease to zero is attenuated until the boundary. All three methods capture this behavior, but we notice that the reaction rates tally dramatically miscalculates the scalar flux at the interface between the source and reflector. This could be due to a sharp increase in scattering and the decrease in mean free path at that location.

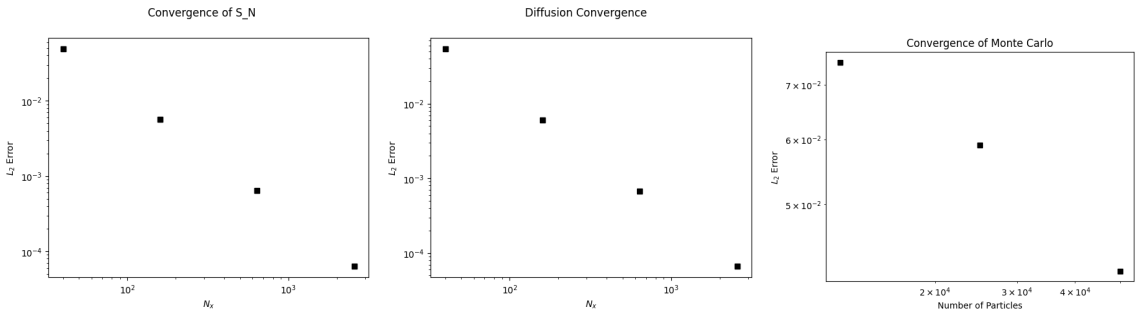

Figure 31: In spite of the reaction rate error at the material discontinuity, the order one-half convergence is upheld for the source reflector system.

3 References

The main references that I consulted for this assignment were the class slides. I also consulted *Computational Methods of Neutron Transport* by Lewis and Miller for some additional advice on how to construct the track length tallies, and I referred to Marvin Adams and Edward Larsen's "Fast Iterative Methods for Discrete-Ordinates Particle Transport Calculations" for the equations needed to build the preconditioner used in deterministic method acceleration. We also based the log-log graph of error on the notion of power law convergence for root finding algorithms like Newton's method as described in William Press et al.'s *Numerical Recipes: The Art of Scientific Computing*. I briefly consulted with Gavin Davis and Abdullah Aljuaid to check on expectations for the simplified Monte Carlo code. Moreover, in past assignments from which my work here was derived I consulted with Max Hoffing, Alex Macris and Harrison Reisinger. The method I used for determining the position of a particle post reflection should be equivalent to that in Braden Pecora's Monte Carlo presentation, and I used resulted presented there as guidance, but I approached this in a loop framework where I incremented until I ran out of mean free paths to travel while reflecting.